Bio-Design and Manufacturing (2023) 6:423–438
https://doi.org/10.1007/s42242-023-00237-3

RESEARCH ARTICLE

Trilayer anisotropic structure versus randomly oriented structure in heart valve leaflet tissue engineering

Yuriy Snyder[1] · Soumen Jana[1]

Received: 1 October 2022 / Accepted: 31 January 2023 / Published online: 17 May 2023

Abstract

It has been hypothesized that leaflet substrates with a trilayer structure and anisotropic mechanical properties could be useful for the production of functional and long-lasting tissue-engineered leaflets. To investigate the influence of the anisotropic structural and mechanical characteristics of a substrate on cells, in this study, we electrospun trilayer anisotropic fibrous substrates and randomly oriented isotropic fibrous substrates (used as controls) from polycaprolactone polymers. Consequently, the random substrates had higher radial and lower circumferential tensile properties than the trilayer substrates; however, they had similar flexural properties. Porcine valvular interstitial cells cultured on both substrates produced random and trilayer cell-cultured constructs, respectively. The trilayer cell-cultured constructs had more anisotropic mechanical properties, 17% higher cellular proliferation, 14% more extracellular matrix (i.e., collagen and glycosaminoglycan) production, and superior gene and protein expression, suggesting that more cells were in a growth state in the trilayer constructs than in the random constructs. Furthermore, the random and radial layers of the trilayer constructs had more vimentin, collagen, transforming growth factor-beta 1 (TGF-ß1), transforming growth factor-beta 3 (TGF-ß3) gene expression than in the circumferential layer of the constructs. This study verifies that the differences in structural, tensile, and anisotropic properties of the trilayer and random substrates influence the characteristics of the cells and ECM in the constructs.

Graphic abstract

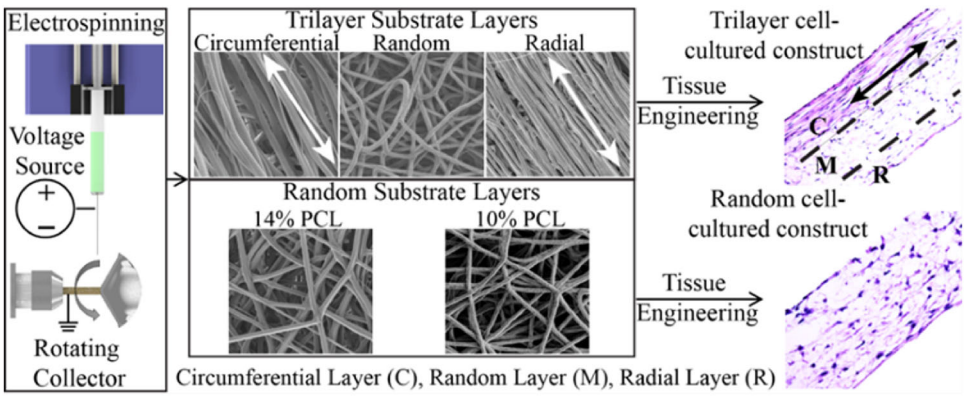

Keywords Heart valve leaflet · Trilayer · Tissue engineering · Fiber · Electrospinning

Introduction

Valvular heart diseases (VHDs) affect a growing number of adult and pediatric patients worldwide [1]. These diseases cause irreparable tissue damage, thus requiring heart valve replacement with either bioprosthetic or mechanical

✉ Soumen Jana
sjgv7@missouri.edu

[1] Department of Bioengineering, University of Missouri, Columbia, MO 65211, USA

valves. Unfortunately, bioprosthetic valves are susceptible to calcification or immune-mediated degradation, and mechanical valves pose thrombotic risks, which require patients to take anticoagulants indefinitely [1, 2]. These valves cannot grow or remodel; thus, pediatric patients must undergo multiple valve replacement surgeries before adulthood until they can accommodate a mechanical valve. Alternatively, tissue-engineered heart valves can be produced from synthetic biodegradable polymer substrates. These substrates can be used as valve replacements and remodel and grow with patients [3].

Heart valve leaflets consist of an organized trilayer extracellular matrix (ECM), i.e., fibrosa, spongiosa, and ventricularis, with valvular interstitial cells (VICs) distributed throughout the structure. The fibrosa, spongiosa, and ventricularis contain circumferentially oriented collagen fibers, randomly oriented glycosaminoglycans (GAGs), and radially oriented elastin, respectively [4, 5]. The trilayer ECM dictates the anisotropic and mechanical characteristics of the tissue and impacts the phenotype of the VICs [6, 7]. Within healthy tissues, approximately 95% of VICs are in a quiescent state, but once exposed to nonnative stresses, these cells activate repair mechanisms and transform into myofibroblast-like phenotypes, which can result in fibrosis, stenosis, calcification, and leaflet retraction [8, 9]. Similarly, heart valve leaflet substrates with nonnative isotropic microstructure and mechanical properties have shown VIC activation and pathogenesis after in vitro or in vivo tissue engineering [10–12]. Therefore, developing substrates for heart valve tissue engineering with a trilayer structure and anisotropic properties similar to native tissues may ensure healthy cell growth and ECM production.

Previously, several trilayer leaflet substrates were produced, including a solid-porous microfabricated polyglycerol sebacate layer sandwiched between the two outer fibrous layers made of electrospun polycaprolactone (PCL) [13], trilayered gel-like nanofibrous substrates consisting of poly(lactic-co-glycolic) acid and poly (aspartic acid) [8], and several trilayered gel/solid-porous substrates that utilized hydrogels or proteins [4, 14]. These trilayer leaflet substrates yielded trilayer cell-cultured constructs that showed resistance to calcification and leaflet retraction [8, 13]. However, many of these trilayer substrates are difficult to produce and require a combination of electrospinning, casting/molding, and hydrogel coatings to yield a trilayer structure and enhance cell responses to the material [15]. Furthermore, casting/molding and hydrogel substrates do not mimic the fibrous structure of native heart valve leaflets [4, 5]. These structural differences between solid-porous or hydrogel substrates and native tissues can cause VIC activation, leading to pathogenesis [16].

Our previous work showed that trilayered tissue constructs developed in vitro from an electrospun nanofibrous trilayer substrate resisted leaflet retraction and had protein expression comparable to native leaflets [17]. Furthermore, trilayer PCL leaflet substrates were implanted into the subcutaneous space of the rat model, yielding tissue constructs with a native-like trilayer structure and protein quantities equivalent to those in a native leaflet [18, 19]. In addition, the trilayer tissue constructs contained many cells in a quiescent state, implying that the substrate structure can impact the phenotype of cells [20]. Despite these efforts, there is no investigation on how trilayer anisotropic leaflet substrates, compared to randomly oriented substrates, influence the cells in promoting native-like trilayer anisotropic structure and properties in tissue-engineered leaflets. Furthermore, it remains unclear whether the cells residing in individual layers of the trilayer cell-cultured constructs exhibit distinct protein and gene expression, which could contribute to the development of functional leaflet constructs.

PCL is readily used in biomedical applications and has been US Food and Drug Administration (FDA)-approved in various implantable medical devices and other biomedical applications. Additionally, this material is easy to electrospin into microfibrous substrates, which have a range of mechanical properties (elastic modulus: 2–20 MPa depending on the molecular weight of PCL) for heart valve tissue engineering and a relatively long biodegradation period [21]. Thus, this material has been used for scaffold fabrication, including for the development of trilayer leaflet substrates intended for in vitro/in vivo tissue engineering [19, 22].

In this study, the electrospinning method was used to produce trilayer anisotropic and randomly oriented substrates from PCL polymer. Porcine VICs (PVICs) were seeded on both substrates and cultured in static conditions for one month, yielding trilayer and random cell-cultured constructs. We examined the effect of the trilayer structure and anisotropic tensile properties of the trilayer substrates on cell proliferation and gene expression, protein expression, ECM production, and the mechanical properties of the trilayer cell-cultured constructs by comparing them with those in random cell-cultured constructs. Finally, we analyzed the morphology of cells and gene expression in each layer of the trilayer cell-cultured constructs.

Materials and methods

Substrate fabrication

Computer-aided design and computer-aided manufacturing (CAD/CAM) software was used to design leaflet-shaped aluminum collectors, and then the collectors were produced through computer numerical control (CNC) machining (Figs. 1a–1c). The collector had three cylindrical holes

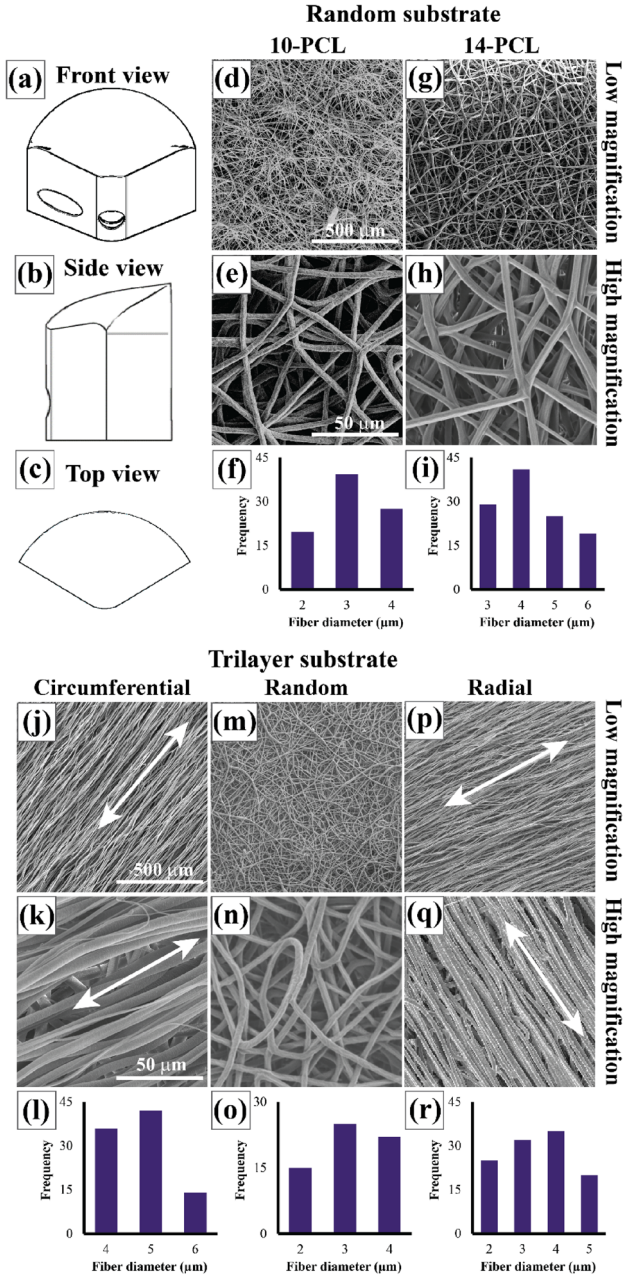

Fig. 1 Schematic of the leaflet collector and structure of each layer of the electrospun random and trilayer substrates. **a**–**c** Front (**a**), side (**b**), and top (**c**) views of the leaflet collector schematic. **d**–**f** Scanning electron microscopy (SEM) images of randomly oriented fibers in the random substrate produced using 10-PCL at low (**d**) and high (**e**) magnification and the fiber diameter distribution (**f**). **g**–**i** SEM images of randomly oriented fibers produced using 14-PCL in the random substrate at low (**g**) and high (**h**) magnification and the fiber diameter distribution (**i**). **j**–**l** SEM images of aligned polycaprolactone (PCL) fibers in the circumferential layer (shown by a double-headed arrow) along the circumferential direction in the trilayer substrate, as shown at low (**j**) and high (**k**) magnifications, and the fiber diameter distribution (**l**). **m**–**o** SEM images of randomly oriented PCL fibers in the random layer of the trilayer substrate at low (**m**) and high (**n**) magnifications and the fiber diameter distribution (**o**). **p**–**r** SEM images of aligned radial PCL fibers in the trilayer substrate at low (**p**) and high (**q**) magnifications and the fiber diameter distribution (**r**). 10-PCL: 10% polycaprolactone solution; 14-PCL: 14% polycaprolactone solution

for mounting to a spindle during electrospinning. Ten percent (0.1 g/mL) and 14% (0.14 g/mL) PCL (MW: 80 KD, Sigma-Aldrich, USA) solutions were prepared in chloroform (Sigma-Aldrich, USA) and separately loaded into syringes. The polymer concentration of an electrospinning solution influences the mechanical properties of an electrospun substrate [23]. Thus, the 10% polycaprolactone solution (10-PCL) was selected for producing the soft and flexible random and radial layers, while the 14% polycaprolactone solution (14-PCL) was selected for the stiff circumferential layer. The syringes were mounted onto a syringe pump (Harvard Apparatus, USA) and placed on a horizontal motion stage. To make the circumferential layer of the trilayer substrate, the 14-PCL solution was electrospun over the collector, rotating about its sagittal axis with the following electrospinning parameters: voltage − 10 kV, solution flow rate − 1.2 mL/h, spinneret–collector distance − 10 cm, and a spin rate of 3000 r/min for 45% of the total electrospinning time. The random layer of the trilayer substrate was made from the 10-PCL solution electrospun over the circumferential layer and collector rotating about its sagittal axis with the following electrospinning parameters: voltage − 14 kV, solution flow rate − 0.7 mL/h, spinneret–collector distance − 12 cm, and a spin rate of 125 r/min for 35% of the total electrospinning time. Finally, the radial layer of the trilayer substrate was produced from the 10-PCL solution and electrospun over the random layer and collector rotating about its coronal axis with the following electrospinning parameters: voltage − 14 kV, solution flow rate − 0.7 mL/h, spinneret–collector distance − 12 cm, and a spin rate of 4000 r/min for 20% of the total electrospinning time. The randomly oriented substrate was produced by electrospinning over the collector rotating along its sagittal axis with the 14-PCL and 10-PCL solutions for 45% and 55% of the total electrospinning time, respectively.

Valvular interstitial cell (VIC) isolation and expansions

Aortic valve leaflets were excised from porcine hearts obtained from a local butcher shop and washed with copious amounts of phosphate-buffered saline (PBS). For PVIC extraction, the leaflets were placed in trypsin solution for 5 min at 37 °C, and the endothelial layer was removed with a sterile cotton swab. Then, the tissue was digested in 0.5% (0.005 g/mL) type I collagenase (Worthington Biochemical, Lakewood, NJ, USA) in PBS for 5 h at 37 °C. Then, the PVICs were isolated by centrifuging the digested tissue for 10 min at 1000 r/min at 4 °C. The cells were resuspended in normal tissue culture (NTC) medium consisting of Dulbecco's modified Eagle's medium (DMEM) supplemented with 10% fetal bovine serum and 1% penicillin–streptomycin and transferred to culture flasks containing NTC medium

and cultured. The PVICs were cultured for 7 days, and the medium was changed every 2 days.

Cell seeding

The random and trilayer substrates were sterilized using 70% ethanol for 6 h at room temperature and then washed with copious amounts of sterile PBS. The substrates were transferred to sterile culture plates and soaked in an NTC medium for 2 days to improve cell attachment. Confluent flasks of PVICs at passage two were trypsinized and resuspended in an NTC medium. The PVICs were seeded onto the substrates at a concentration of 5×10^5 cells/cm^2. The cell-seeded substrates were allowed to sit for 30 min to enable cell adhesion before adding NTC medium to each sample well. The samples were cultured for 30 days with NTC medium changed every 3 days.

Scanning electron microscopy

Scanning electron microscopy (SEM) imaging was performed on 3 mm×3 mm square pieces of random and trilayer substrates or random and trilayer cell-cultured constructs (n=2 of each). Cell-cultured constructs were prepared by fixation in 10% formalin and freeze-drying. The samples were mounted onto SEM stubs with either the circumferential, random, or radial layer exposed. They were then sputter-coated with 25 nm of platinum before imaging in an SEM (FEI Company, USA) at 10 kV. The SEM showed the properties of the samples, such as the orientation of fibers, the morphology of the cells, and the fiber diameter and pore size—measured using the SEM software.

Mechanical testing

A tensile tester (TestResources, Canada) was used to measure the displacement, stress, and strain of substrates and cell-cultured constructs (n=5 of each) cut along their circumferential or radial direction (n=5 of each) as described previously [18, 24]. Additionally, several cell-cultured constructs (n=5) were soaked in 5.25% sodium hypochlorite on an orbital shaker for 4 h to remove the ECM materials to obtain leftover substrates. The leftover substrates were prepared for tensile testing according to the same specifications as the substrates and cell-cultured constructs. Briefly, the samples were cut into 2 mm×10 mm radial and circumferential strips, and their thicknesses were measured using a caliper gauge (Mitutoyo, Japan). The samples were then sandwiched between two paper window frames with dimensions of 5.5 mm×5.5 mm and glued. The frames were mounted into the tensile tester, and the ends of the frame were cut. Slack was removed from the sample by applying a preload of 0.01 N. The tensile test of the substrates was conducted under dry conditions. However, cell-cultured constructs remained hydrated in PBS during the tensile testing. Testing was conducted at a head rate of 6 mm/s. The tensile modulus and yield stress were calculated using the measured displacement, stress, and strain data. The circumferential elastic modulus or ultimate tensile strength was divided by the radial elastic modulus or ultimate tensile strength to calculate the anisotropic ratios of the elastic modulus and ultimate tensile strength, respectively [13].

The flexural moduli of the substrates and cell-cultured constructs (n=5 of each type) were measured in a horizontal tensile tester (TestResources, Canada) according to methods established in the previous literature [25, 26]. Briefly, the samples were cut into 2 mm×8 mm circumferential strips, mounted onto custom cylindrical holders, and placed in the tensile tester. The samples were compressed at a head rate of 1 mm/s, and the force and deflation of the samples were recorded. Linear flexural bending theory was applied to calculate the flexural modulus of the samples.

Protein quantification assays and mass spectrometry

Before protein extraction, the cell-cultured constructs (n=3 of each type) were cut into 3 mm×3 mm sections and weighed. For collagen extraction, samples were placed in collagen extraction solution (0.5 mol/L acetic acid+100 U/mL pepsin in water) overnight at 37 °C. Then, a Sircol insoluble collagen assay kit (Biocolor Ltd., UK) was used to measure the amount of collagen in the constructs according to the protocols provided by the company. The absorbance at 550 nm wavelength was measured with a microplate spectrophotometer (BioTek, USA), and the collagen concentration was determined by comparing the absorbance to a standard curve obtained using a set of collagen solutions of known concentrations. For glycosaminoglycan (GAG) extraction, the samples were placed in a GAG extraction solution (4 mol/L guanidine-HCl and 0.5 mol/L sodium acetate in water) overnight at 8 °C. Then, a Sircol GAG assay kit (Biocolor Ltd., UK) was used to measure the amount of GAG in the constructs according to the protocols provided by the company. The spectrophotometer measured the absorbance at 656 nm wavelength. The GAG concentration was determined by comparing the measured absorbance to a standard curve produced using standard GAG solutions of known concentration.

For mass spectrometry (MS), proteins were extracted from 50 mg of the trilayer and random cell-cultured constructs using sodium dodecyl sulfate (SDS)/acetone precipitation and then digested using subsequent alkylation and trypsinization [27, 28]. Then, peptides were desalted and concentrated using C18 tips according to the manufacturer's protocols (Pierce/Thermo Scientific, USA). The peptides were resuspended, and 1 μL was injected directly onto an analytical

column packed with Waters BEH-C18, 1.7 μm reversed-phase resin. Peptides were separated and eluted from the analytical column (20 cm long × 75 μm inner diameter) with a gradient of acetonitrile at 300 nL/min. MS analysis was performed on a mass spectrometer (Bruker, USA) operating in positive mode. Data were collected over a range of 100 to 1700 m/z at a resolution of 10,000 counts/s with a minimum threshold of 250 counts/s. A charge-state-based rolling collision energy table was used from 76% to 123% of 42.0 eV. An active exclusion/reconsideration precursor method with release after 0.4 min was used. If the precursor (within a mass width error of 0.015 m/z) was >4X signal intensity in subsequent scans, a second MS/MS spectrum was collected. The isolation width was set to 2 m/z (<700 m/z) or 3 m/z (800–1500 m/z). The acquired data were submitted to PEAKS X+ for protein identification [29].

Histology and immunostaining

The random and trilayer cell-cultured constructs were fixed in 10% formalin for 24 h and then washed in PBS. The constructs were cut into radial and circumferential sections and embedded in Tissue-Tek® O.C.T. Compound at −20 °C (Sakura, Alphen den Rijn, The Netherlands). The samples were sectioned at 10 μm and mounted onto glass slides. The sections were thawed for 20 min before staining with hematoxylin and eosin (H&E, Thermo Fisher Scientific, USA), Masson's trichrome (Thermo Fisher Scientific, USA), Alcian blue (Thermo Fisher Scientific, USA), and von Kossa (Abcam, USA) to show the general morphology of the cells and tissues, collagen fibrils, GAG, and calcium nodules, respectively. Images were obtained using a Zeiss Axiovert 200 M with an ORCA-ER camera at 20× magnification.

Furthermore, radial and circumferential sections of random and trilayer cell-cultured constructs were prepared for immunohistochemical analysis using antibodies against vimentin (ab92547, Abcam, USA) and α-smooth muscle actin (α-SMA) (ab124964, Abcam, USA). The sections were thawed for 20 min, and the O.C.T. compound was removed. Goat serum was used to permeabilize and block the samples. Then, the sections were incubated in the primary antibody at 4 °C for 12 h and then incubated in the secondary antibody for 2 h. The slides were rinsed with PBS between each step. Finally, a glass coverslip was mounted onto the slide using DAPI. The slide sections were imaged using a Leica GSD microscope.

Random and trilayer cell-cultured constructs were cut into 3 mm × 3 mm sections, and the circumferential layer was separated from the radial/random layers. As described above, the samples were dehydrated, permeabilized, blocked, and stained with a vimentin marker. Then, the samples were counterstained using Hoechst 33342 (Thermo Fisher, USA) according to the manufacturer's protocols. The samples were washed with PBS, placed into a glass-bottom dish with either the radial or circumferential surface facing up and imaged with a spectral confocal microscope (Lecia, Germany).

Proliferation test

PVICs (300,000/substrate) were seeded onto random and trilayer substrates (n=4 of each) and cultured in NTC media. The cellular proliferation on the substrates was measured using an alamarBlue assay at 1-, 3-, 8-, and 14-day time points. A microplate spectrophotometer (BioTek, USA) was used to record the absorbance of the samples at 570 and 600 nm wavelengths at each time point. The results were compared to an absorbance calibration curve produced using known cell numbers to determine the cell number on the substrates.

Gene expression

RNAs from the random and trilayer cell-cultured constructs (n=5 of each) were collected using the QIAshredder spin column (QIAGEN, Germany) and RNeasy mini kit (QIAGEN, Germany) and their supplied instructions [18, 30]. Briefly, a combination of guanidine thiocyanate (RLT) buffer (supplied with the kit) with β-mercaptoethanol (Sigma-Aldrich, St. Louis, MO, USA) and stirring was used to lyse the samples. Additionally, the samples were homogenized further by using the QIAshredder spin column. Finally, the RNeasy mini kit was used to isolate the RNA from the samples. The isolated RNA was transcribed to cDNA using a high-capacity cDNA reverse transcription kit and the supplied instructions [18]. The cDNA transcripts were then probed with TaqMan assays for α-smooth muscle actin (ACTA2, Ss04245588_m1), vimentin (VIM, Ss04330801_gH), type I collagen (COL1A1, Ss03373341_g1), bone gamma-carboxyglutamate protein (BGLAP, Ss03373655_s1), transforming growth factor-beta 1 (TGF-β1, Ss04955543_m1), transforming growth factor-beta 3 (TGF-β3, Ss03394351_m1), and β-actin (ACTβ, Ss03376563_uH) as a normalizer gene using a TaqMan universal PCR master mix (Applied Biosystems, USA). Amplification and data collection were performed in an AriaMx real-time PCR system (Agilent, USA) using our previously described conditions [17]. Finally, the target gene data were normalized and evaluated using the comparative cycle threshold (Ct) method. The gene expression in the circumferential and random/radial layers of the trilayer cell-cultured construct was assessed using the same method.

Statistical analysis

All numerical data are expressed as the mean±standard deviation (SD). Unpaired t tests and one-way analysis of

variance (ANOVA) with Tukey's post hoc tests were applied to 2-group and 3-group comparisons, respectively. Statistical significance was established at a two-tailed $p<0.05$.

Results and discussion

Structure of the random and trilayer leaflet substrates

In this study, we compared the usefulness of random and trilayer substrates for heart valve tissue engineering by examining the impact of the substrate structure on PVICs during their respective construct engineering [17, 31]. The polymer concentration of an electrospinning solution affects the mechanical and structural characteristics of a substrate [23]. Thus, the trilayer substrates were electrospun with 14% PCL (14-PCL) for the stiff circumferential layer and 10% PCL (10-PCL) for the soft random and radial layers. Furthermore, the electrospinning times were adjusted so that the trilayer substrate had a total thickness of ~0.3 mm with circumferential, random, and radial layer thicknesses of ~0.135 mm, ~0.105 mm, and ~0.06 mm, respectively, mimicking the layer thickness percentages of the trilayer native leaflets—45% circumferential, 35% random, and 20% radial [13, 32]. To develop random substrates with similar layer thicknesses to the trilayer substrates, the electrospinning times were adjusted to produce about 0.3-mm-thick random substrates with an about 0.135-mm-thick 14-PCL layer and an about 0.165-mm-thick 10-PCL layer, which constituted 45% (same as the circumferential layer of a trilayer substrate) and 55% (same as the random/radial layers of a trilayer substrate) of the total thickness, respectively.

Cell behavior depends on several characteristics of the substrate, including fiber orientation and diameter and pore size [18]. Thus, the substrate structure and fiber orientations were verified using SEM imaging at high and low magnifications. The random substrate had randomly oriented fiber layers electrospun from 10-PCL and 14-PCL, with fiber diameters of 2–4 μm and 3–6 μm and pore sizes of 14–18 μm and 16–20 μm measured using SEM imaging software, respectively (Figs. 1d–1i). In the trilayer substrates, a highly aligned circumferentially oriented fiber was observed in the circumferential layer with fiber diameters of 4–6 μm and pore sizes of approximately 10 μm (Figs. 1j–1l). The random layer had a random fiber orientation with fiber diameters of 2–4 μm and pore sizes of 14–18 μm (Figs. 1m–1o). Finally, the radial layer had a highly aligned and radially oriented fiber structure with fiber diameters of 2–5 μm and pore sizes of approximately 10 μm (Figs. 1p–1r). The layers produced from the 14-PCL solution had greater fiber diameters than those produced from the 10-PCL solution in the random and trilayer substrates [33]. Additionally, layers with aligned fibers exhibited smaller pore sizes due to the tendency for aligned fibers to compact at high collector spin speeds [12]. However, the average diameter of VICs is approximately 7–8 μm, so pore sizes of 10 μm or greater are adequate for ensuring cell infiltration into the substrates [34, 35].

Mechanical properties

Heart valve leaflets are highly anisotropic and flexible and have large tensile properties along the circumferential direction and relatively low tensile properties in the radial direction [36]. These properties dictate the leaflet function and the phenotypes of the VICs in the leaflets [37]. Therefore, the tensile and flexural properties of the random and trilayer substrates and their cell-cultured constructs were measured with a tensile tester. The stress–strain curves in the circumferential and radial directions of the random substrate and cell-cultured constructs differed significantly from the curves of the trilayer substrate and cell-cultured constructs (Figs. 2a and 2b). The trilayer substrate and cell-cultured constructs had several peaks indicating individual layers breaking during the tensile testing.

The tensile moduli and strengths of the random substrates were (7.75±0.87) MPa and (1.85±0.22) MPa in the circumferential direction and (7.31±0.56) MPa and (1.72±0.19) MPa in the radial direction. The tensile moduli and strengths of the trilayer substrates were (10.45±0.85) MPa and (2.23±0.42) MPa in the circumferential direction and (2.89±0.17) MPa and (1.06±0.21) MPa in the radial direction. The random substrates had a lower (statistically significant, $p<0.05$) circumferential tensile modulus than the trilayer substrates (Figs. 2c and 2d). Electrospun fiber aligned parallel to the direction of a tensile test, such as the circumferential layer in the trilayer substrate, had higher mechanical properties than randomly oriented fibers [23]. In contrast, random substrates had a greater radial tensile modulus and strength (statistically significant, $p<0.005$) than trilayer substrates. Trilayer substrates are primarily composed of circumferentially oriented fibers in the circumferential layer, which do not contribute significantly to the tensile properties in the radial direction [38]. Comparatively, the thinner random layer of the trilayer substrates contains randomly oriented fibers that contribute a small amount to the tensile properties of the substrate in both the radial and circumferential directions. Conversely, the random substrates contain only randomly oriented fibers that give isotropic tensile properties to the substrate, yielding similar tensile properties in the radial and circumferential directions [12], leading to higher tensile properties in their radial direction compared to those in the radial direction of trilayer substrates.

After cell culture, the tensile moduli and strengths of the random cell-cultured constructs were (7.72±0.26) MPa and (1.69±0.13) MPa in the circumferential direction and

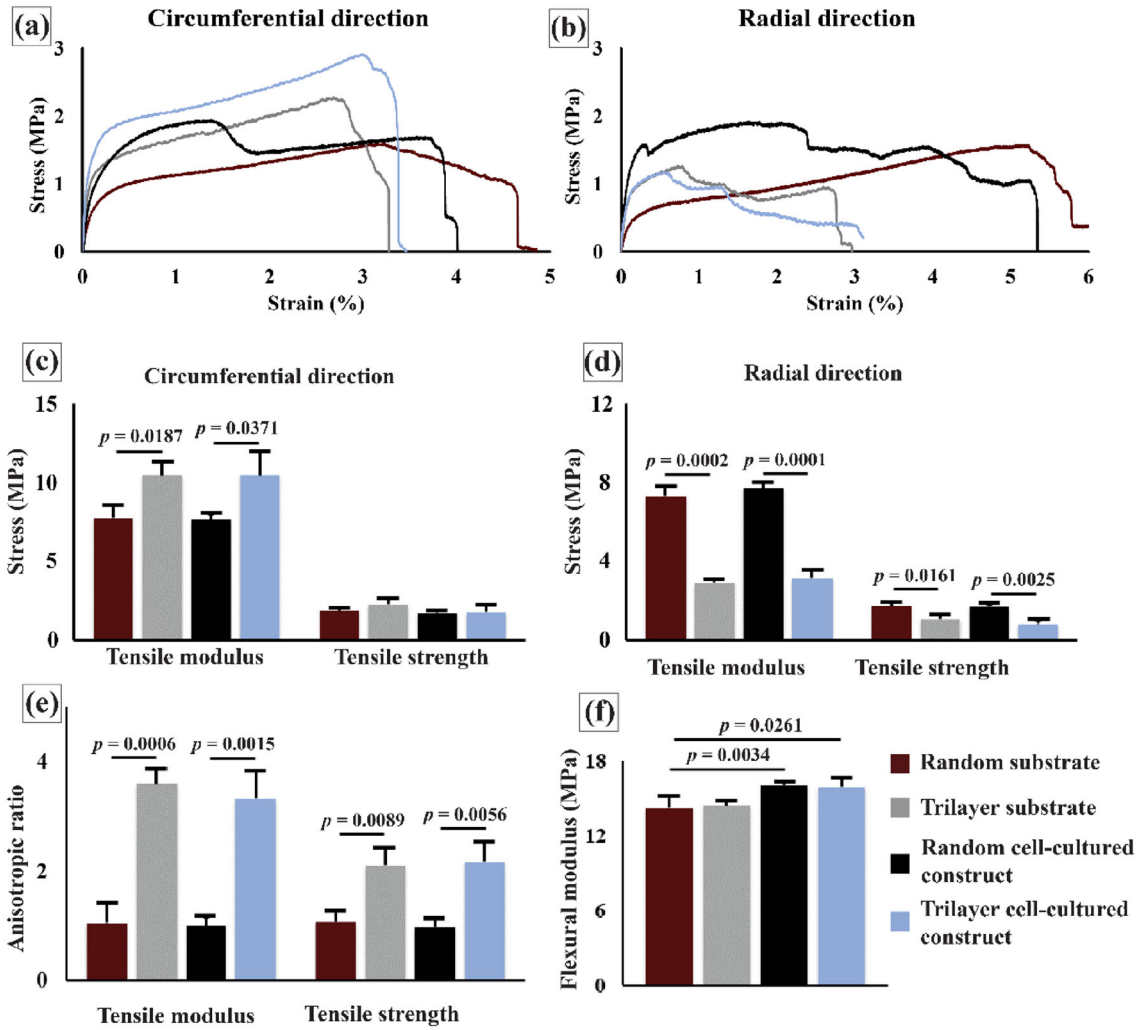

Fig. 2 Mechanical testing of the random and trilayer substrates and cell-cultured constructs. **a**, **b** Stress–strain curves of the random and trilayer substrates and cell-cultured constructs in the circumferential (**a**) and radial (**b**) directions. **c**, **d** Tensile moduli and strengths of the random and trilayer substrates and cell-cultured constructs in the circumferential (**c**) and radial (**d**) directions, respectively. **e** The anisotropic ratios (circumferential/radial) of the tensile moduli and strengths of the random fiber and trilayer substrates and cell-cultured constructs. **f** The flexural moduli of the random and trilayer substrates and cell-cultured constructs

(7.63±0.38) MPa and (1.70±0.21) MPa in the radial direction (Figs. 2c and 2d). The circumferential and radial tensile moduli of the random cell-cultured constructs were statistically equivalent to those of the original random substrates. Trilayer cell-cultured constructs had tensile moduli and strengths of (10.47±1.55) MPa and (1.75±0.57) MPa in the circumferential direction and (3.14±0.46) MPa and (0.80±0.19) MPa in the radial direction. There was no significant difference in the tensile properties of the trilayer substrates and trilayer cell-cultured constructs.

Despite one month of cell culture that produced ECM materials inside the substrates, the random and trilayer cell-cultured constructs exhibited statistically equivalent tensile properties to their respective substrates. The degradation of the electrospun fibers in the cell-cultured constructs and the ECM materials produced by the cells could have impacted the tensile properties of the cell-cultured constructs [13, 39]. Thus, the ECM materials and cells were removed from the random and trilayer cell-cultured constructs to produce leftover random and trilayer substrates, which were then tested to measure their tensile properties. The tensile moduli and strengths of the leftover random substrates were (7.57±0.32) MPa and (1.57±0.16) MPa in the circumferential direction and (7.66±0.34) MPa and (1.51±0.11) MPa in the radial direction. The leftover trilayer substrates had tensile moduli and strengths of (9.96±0.46) MPa and (2.08±0.96) MPa in the circumferential direction and (2.84±0.14) MPa and (0.79±0.21) MPa in the radial direction. In both cases, the

tensile properties of the leftover random or trilayer substrates were lower than those of the random or trilayer cell-cultured constructs and random or trilayer substrates, but their differences were not significantly different. The neo-ECM produced by VICs in the random and trilayer cell-cultured constructs had significantly lower tensile properties than electrospun PCL fibers, and its contribution toward the tensile properties of the constructs was compromised by the degradation of random and trilayer substrates, so the random and trilayer cell-cultured constructs exhibited statistically equivalent tensile properties to their respective substrates [23, 40].

The tensile moduli and strengths of the random and trilayer cell-cultured constructs in the circumferential direction were significantly different (statistically significant, $p<0.05$). The aligned circumferential electrospun fibers in the trilayer cell-cultured constructs are responsible for these higher tensile properties compared to the random cell-cultured constructs. However, the tensile modulus and strength of the trilayer cell-cultured constructs in the radial direction were lower than those observed in the random cell-cultured constructs (statistically significant, $p<0.05$). These differences in tensile properties between the two constructs in the radial direction are caused by randomly oriented electrospun fibers in the random cell-cultured constructs with respect to the circumferentially oriented electrospun fiber in the trilayer cell-cultured constructs, which has a small contribution to the tensile properties in the radial direction [12].

The tensile modulus and strength anisotropic ratios were 1.06±0.35 and 1.07±0.20 for the random substrates and 3.61±0.87 and 2.11±0.31 for the trilayer substrates, respectively (Fig. 2e). After tissue engineering, the tensile moduli and strength anisotropic ratios were (0.98±0.16) MPa and (1.01±0.13) MPa for the random cell-cultured constructs and (3.33±0.50) MPa and (2.18±0.35) MPa for the trilayer cell-cultured constructs, respectively. The tensile modulus and strength anisotropic ratios of the random and trilayer cell-cultured constructs did not differ from their respective substrates (statistically significant, $p<0.05$). However, both the tensile modulus and strength anisotropic ratios of the random and trilayer substrates were significantly different ($p<0.05$). Similarly, the anisotropic ratios of the random and trilayer cell-cultured constructs were significantly different ($p<0.05$). Thus, the trilayer substrates and cell-cultured constructs were more anisotropic than random substrates and cell-cultured constructs.

Trilayer cell-cultured constructs were anisotropic and had tensile properties more comparable to native heart valve leaflets than bioprosthetic valves. Clinically used bioprosthetic valves, such as St Jude Epic bioprostheses, have high anisotropic properties. However, chemical fixation causes their tensile properties—circumferential and radial moduli of 101.99 MPa and 9.18 MPa, respectively, which are significantly higher than those of native tissues (circumferential and radial moduli of 15.34 MPa and 1.98 MPa, respectively) [41]. Furthermore, trilayer cell-cultured constructs supported cell proliferation and ECM production; however, bioprosthetic valves cannot support cell growth or remodeling [21].

The flexural moduli of the random and trilayer substrates were (14.26±0.45) MPa and (14.45±0.36) MPa, respectively (Fig. 2f). After tissue engineering, the random and trilayer cell-cultured constructs had flexural moduli of (16.13±0.25) MPa and (15.97±0.67) MPa, respectively. The flexural moduli of the random and trilayer cell-cultured constructs increased compared to their respective substrates (statistically significant, $p<0.05$). Furthermore, there was no difference in the flexural moduli between the random and trilayer substrates. Likewise, the flexural moduli of the random and trilayer cell-cultured constructs were not significantly different. The flexural properties of a fibrous substrate are related to several factors, including pore size and diameter [42]. Both random and trilayer substrates had similar pore sizes and fiber diameters, which could have been responsible for the similar flexural properties in their respective cell-cultured constructs.

Cell proliferation

PCL is a biocompatible polymer that obtained FDA clearance for use in multiple implantable medical devices, including substrates for tissue engineering. Substrates made from PCL with a trilayer structure may promote greater cell proliferation [43, 44]. Thus, an alamarBlue cell proliferation assay was conducted to compare cell viability and proliferation on random and trilayer substrates over a 14-day cell culture. Initially, there was no difference in cellular proliferation on the two substrates, suggesting that both supported a similar amount of cell adhesion. However, after 14 days of cell culture, the trilayer cell-cultured constructs showed 17% greater cellular proliferation than the random cell-cultured constructs (Fig. 3a). These results suggest that the trilayer structure and mechanical anisotropic properties of the trilayer substrate may positively impact cell proliferation. VICs have been shown to proliferate faster on aligned fiber substrates than on substrates with random fiber orientations because cells preferentially migrate and proliferate along the direction of the aligned fiber [45–47]. Therefore, the VICs seeded on the radial or circumferential sides of the trilayer substrates could have responded positively to the aligned fiber structures. SEM imaging showed that the surfaces of the random and trilayer cell-cultured constructs had confluent ECMs (Figs. 3b–3g).

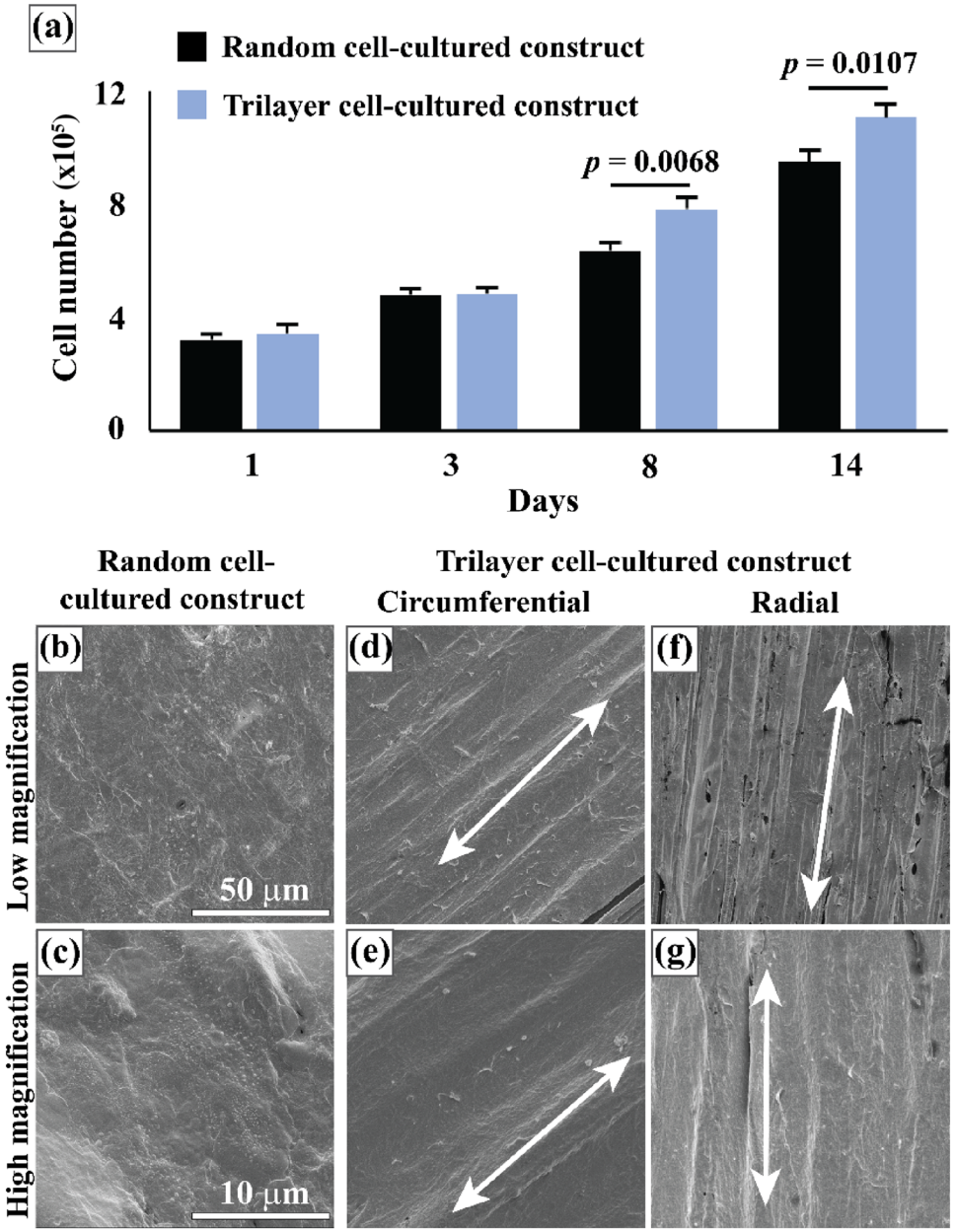

Fig. 3 Cellular proliferation and extracellular matrix (ECM) production on the random and trilayer cell-cultured constructs. **a** Cell numbers on the random and trilayer cell-cultured constructs after 1, 3, 8, and 14 days of cell culture. **b**, **c** Images of the random cell-cultured construct surface after one month of tissue engineering at low (**b**) and high (**c**) magnifications. **d**–**g** Images of the circumferential (**d**, **e**) and radial (**f**, **g**) surfaces of the trilayer cell-cultured constructs after a one-month static culture

Histology

The orientation of the fibers within electrospun substrates influences the orientation and morphology of proliferating cells and their produced ECM [48, 49]. Random substrates had a structure with random fiber orientations, while the trilayered substrate had circumferential, random, and radial fiber orientations in three layers mimicking the native leaflet tissue structure. Thus, the cell-cultured constructs were stained to verify the orientation of cells and their produced ECM components and compare the extent of cell proliferation and ECM production. H&E-stained sections of the random cell-cultured constructs had randomly oriented cells and collagen fibrils throughout the construct (Fig. 4a). Radial and circumferential sections of the trilayer cell-cultured constructs stained with H&E showed an evident trilayer structure with distinct regions of aligned and randomly oriented cells and collagen fibrils (Figs. 4b and 4c). It was apparent that there were more cell proliferation and ECM production in the trilayer cell-cultured constructs than in the random cell-cultured constructs. Furthermore, the circumferential layer of the trilayer cell-cultured constructs had more cell proliferation and ECM production than the other two layers. The aligned fibrous layers and anisotropic properties of the trilayer cell-cultured constructs may have encouraged greater

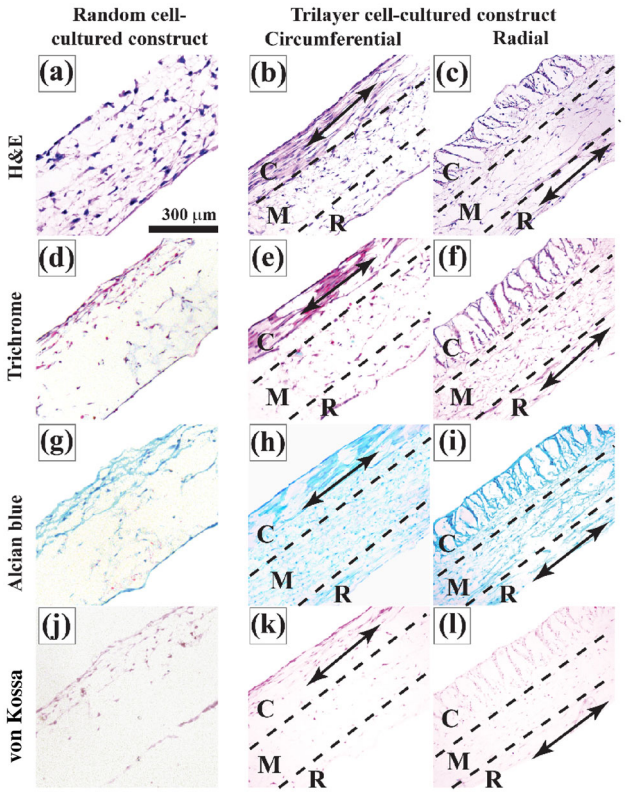

Fig. 4 Histological images of random and trilayer cell-cultured constructs developed after one month of static culture. **a–c** H&E-stained random (**a**), circumferential (**b**), and radial (**c**) cross sections of cell-cultured constructs show aligned circumferential (C) and radial (R) layers and a randomly oriented middle (M) layer. **d–f** Masson's trichrome-stained random (**d**), circumferential (**e**), and radial (**f**) cross sections of cell-cultured constructs show aligned circumferential (C) and radial (R) layers and a randomly oriented middle (M) layer. **g–i** Alcian blue-stained random (**g**), circumferential (**h**), and radial (**i**) cross sections of cell-cultured constructs show aligned circumferential (C) and radial (R) layers and a randomly oriented middle (M) layer. **j–l** von Kossa-stained random (**j**), circumferential (**k**), and radial (**l**) cross sections of cell-cultured constructs show aligned circumferential (C) and radial (R) layers and a randomly oriented middle (M) layer. Alignment in the circumferential and radial directions can be observed in the C and R layers (shown with a double-headed arrow). Dots in the R layer of the circumferential cross sections and the C layer of the radial cross sections show the alignment perpendicular to the cross section. The random middle (M) layer showed a random orientation

cell proliferation and the development of ECM materials by the cells [50].

Images of Masson's trichrome-stained random cell-cultured constructs showed that collagen fibril development mainly occurred in the outermost regions of the constructs and had a random orientation (Fig. 4d). Conversely, radial and circumferential sections of the trilayer cell-cultured constructs had aligned collagen fibrils in the radial and circumferential layers (Figs. 4e and 4f). The middle layer had randomly oriented collagen fibrils. Native leaflets have the most collagen fibrils in the circumferentially oriented fibrosa layer [51]. Similarly, most of the collagen fibrils were in the circumferential layer of the trilayer cell-cultured construct.

In native leaflets, the spongiosa layer is composed of mostly randomly oriented GAG that acts as a cushion between the two outer layers [4, 5]. Thus, Alcian blue was used to stain the cell-cultured constructs to confirm the presence of GAG. Sections of random cell-cultured constructs had GAG production mainly in the outer regions of the structure (Fig. 4g). Conversely, the trilayer cell-cultured constructs had a more uniform GAG distribution throughout the structure than the random cell-cultured constructs (Figs. 4h and 4i). One possible reason for this observation is that GAG production is often elevated in anisotropic multilayer substrates because GAG provides cushioning between the two outer layers of the substrates [4, 52].

Heart valve calcification obstructs leaflet function and is one of the primary causes of heart valve failure. This illness can occur in leaflet tissues when activated VICs are exposed to nonnative stresses and bone transcription factors that lead to cell transdifferentiation into bone phenotypes [21]. Thus, the cell-cultured constructs were stained with von Kossa to show if osteogenic deposits formed in the constructs. Neither random nor trilayer cell-cultured constructs formed calcium deposits (Fig. 4j-4l).

Quantification of matrix components

Collagen, GAG, and elastin comprise the native leaflet ECM and affect its structural and mechanical attributes. Collagen and elastin dictate the load-bearing capacity and elasticity of the tissue, respectively, while GAG acts as a cushion between these fibrous proteins [53, 54]. Therefore, we conducted biochemical assays to determine the quantity of collagen and GAG in the random and trilayer cell-cultured constructs (Fig. 5a). Trilayer cell-cultured constructs contained more collagen and GAG than the random tissue-engineered constructs. Fiber alignment and anisotropic properties in cell-seeded substrates promote cell elongation and accelerate cell migration, leading to greater production of ECM materials [55, 56]. Similarly, the trilayer cell-cultured constructs have anisotropic properties and are composed of layers with aligned fiber structures that could have promoted collagen and GAG production.

Leaflet function depends on the expression of several proteins responsible for dictating cellular processes. Gamma actin (ACTG1) and tubulin are essential cytoskeletal proteins associated with cell motility and mitosis, respectively [57, 58]. Phosphoglycerate kinase 1 (PGK-1) is an important enzyme for the production of adenosine triphosphate (ATP) during glycolysis and is an indicator of healthy cell metabolism [59]. Histones are proteins that protect DNA from damage and are associated with the presence of cellular DNA [60]. Thus, protein mass spectrometry was used

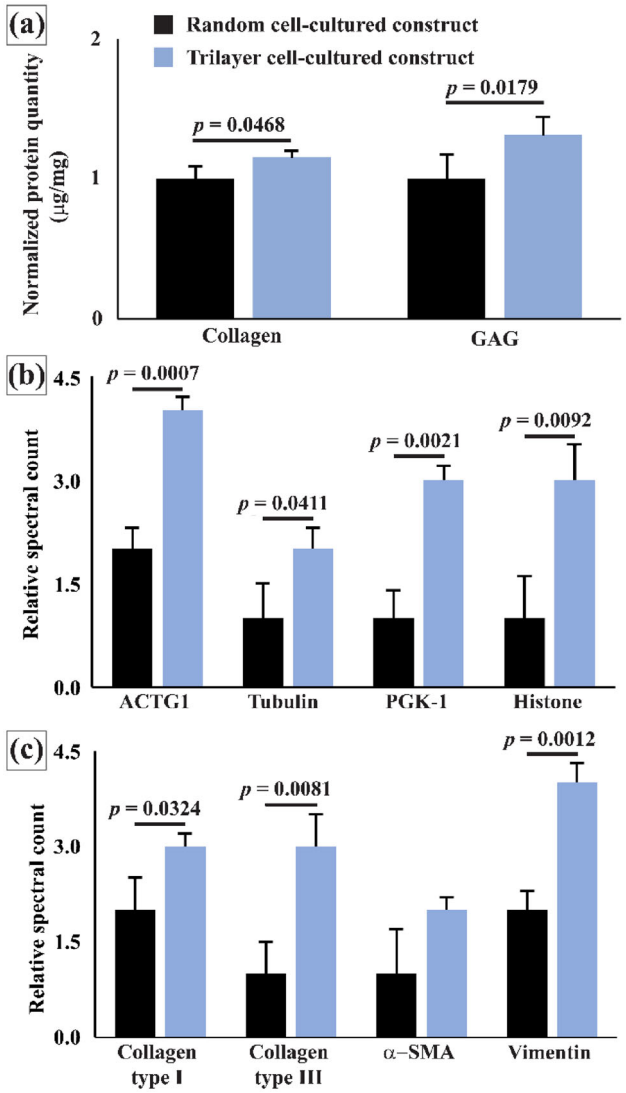

Fig. 5 Quantification of extracellular matrix (ECM) components and relative protein expression in the random and trilayer cell-cultured constructs. **a** Normalized collagen and glycosaminoglycan (GAG) protein quantities in random fiber and trilayer cell-cultured constructs. **b** Relative protein expression of gamma actin (ACTG1), tubulin, phosphoglycerate kinase 1 (PGK-1), and histones in the random and trilayer cell-cultured constructs. **c** Relative protein expression of collagen type I, collagen type III, α-smooth muscle actin (α-SMA), and vimentin in the random and trilayer cell-cultured constructs

to analyze the relative quantities of several proteins associated with intercellular processes in the random and trilayer cell-cultured constructs (Figs. 5b and 5c). The trilayer cell-cultured constructs had significantly higher quantities of ACTG1, PGK-1, tubulin, and histones than random cell-cultured constructs (Fig. 5b). Low expression of ACTG1 is associated with over a dozen cardiovascular disorders and poor cell motility [57, 61]. Thus, high expression of ACTG1 in the trilayer cell-cultured constructs may indicate cell resistance to pathogenesis and high cell motility. The high expression of PGK-1 and tubulin in the trilayer cell-cultured constructs could represent high cell proliferation and healthy cell metabolism in the construct [58, 59, 62]. The relatively large presence of histones in trilayer cell-cultured constructs compared to the random cell-cultured constructs could suggest that a large amount of compact chromosomal cell DNA was present in the constructs [60, 63].

Heart valves are primarily composed of collagen types I and III, which are responsible for providing structural support and flexibility to the tissue. Furthermore, while in a growth state, VICs express high levels of α-SMA and vimentin, enabling ECM material development [21]. Thus, the relative expression of ECM proteins such as collagen types I and III, α-SMA, and vimentin was also verified with protein mass spectrometry. The trilayer cell-cultured constructs had a higher relative expression of collagen type I, collagen type III, and vimentin than the random cell-cultured constructs (Fig. 5c). However, there was no difference in α-SMA expression in these two cell-cultured constructs. The higher expression of both collagen types in the trilayer cell-cultured constructs could be due to cells responding positively to the trilayer structure and producing more collagen fibrils, as shown in the previous sections. The higher vimentin protein expression in the trilayer cell-cultured constructs may have indicated that many cells were in a growth state. The anisotropic properties of the trilayer cell-cultured constructs could have caused greater expression of vimentin and collagen type I [64].

Gene expression and immunostaining

VICs in healthy native tissues maintain a quiescent state, regulate valvular homeostasis, and express moderate levels of vimentin [65]. However, upon exposure to nonnative stresses (e.g., tissue damage), VICs can transform into α-SMA-positive myofibroblasts, which produce collagen (COLA1), express high levels of vimentin, and initiate growth and repair of the tissue [65, 66]. Furthermore, TGF-β1 and TGF-β3 are upregulated in VICs in a growth state and control cell proliferation, migration, and cytokine secretion [67]. In addition, cell gene expression of BGLAP may indicate cell differentiation into osteoblast phenotypes that may lead to eventual calcification [68]. Therefore, we conducted reverse transcription polymerase chain reaction (RT–PCR) to determine the gene expression of α-SMA, VIM, COLA1, TGF-β1, TGF-β3, and BGLAP in PVICs cultured on random or trilayer cell-cultured constructs.

The VICs in the trilayer cell-cultured constructs had higher gene expression of VIM, COLA1, TGF-β1, and TGF-β3 than those in random cell-cultured constructs, but there was no difference in α-SMA or BGLAP gene expression (Figs. 6a and 6b). These observations suggest that more

VICs were in a growth state in the trilayer cell-cultured constructs than in the random cell-cultured constructs [65, 66]. The high collagen expression in the trilayer cell-cultured constructs is consistent with the collagen protein quantification results described in the previous section. The collagen expression results suggested that the anisotropic properties of the trilayer structure encouraged greater collagen production [64]. Furthermore, high TGF-β1 and TGF-β3 gene expression in the trilayer cell-cultured constructs confirmed that VICs produced more growth factors for cell proliferation and migration. The higher growth factor expression in the trilayer cell-cultured constructs could be due to VICs producing growth factors in response to the anisotropic properties of the cell-cultured constructs [13, 54, 55]. Thus, the anisotropic structural and mechanical properties of the trilayer cell-cultured constructs may cause cells to produce more growth factors. Furthermore, TGF-β1 and TGF-β3 are essential for cell proliferation and ECM production, but TGF-β1 gene expression may contribute to fibrosis by regulating processes that produce excessive collagen type I. Conversely, TGF-β3 may promote cell migration and mediate biochemical mechanisms that prevent excessive collagen type I production [69]. TGF-β3 gene expression was significantly higher than TGF-β1 gene expression (statistically significant, $p<0.05$) in the trilayer cell-cultured constructs, indicating that the trilayer structure could resist fibrosis. Additionally, the random or trilayer cell-cultured constructs expressed negligible amounts ($C_p>34$) of BGLAP, suggesting that neither construct posed a risk of calcification.

The random and trilayer cell-cultured constructs were stained with vimentin (green) and α-SMA (red) protein markers to verify the state of the cell-cultured constructs and compare their protein expression with the gene expression described above. Vimentin and α-SMA protein expression was detected in the random cell-cultured constructs (Figs. 6c and 6d), but the trilayer cell-cultured constructs had greater protein expression (Figs. 6e–6h). The random cell-cultured constructs showed more vimentin and α-SMA protein expression in the outer regions, indicating that remodeling did not occur equally throughout the entire structure. Vimentin and α-SMA protein expression in the trilayer cell-cultured constructs occurred mainly in the circumferential layer but was visible in other regions. Vimentin and α-SMA proteins maintain the structure of cells and indicate VIC activation, respectively [65]. Furthermore, cells cultured on electrospun substrates with aligned fibers exhibit an elongated morphology parallel to the fiber and express more vimentin to maintain their morphology [65, 66, 70]. Thus, the greater production of vimentin proteins by the VICs in trilayer cell-cultured constructs than in random cell-cultured constructs could be due to the VICs exhibiting an elongated morphology in the aligned layers of the trilayer cell-cultured constructs. Additionally, there were significantly more cell

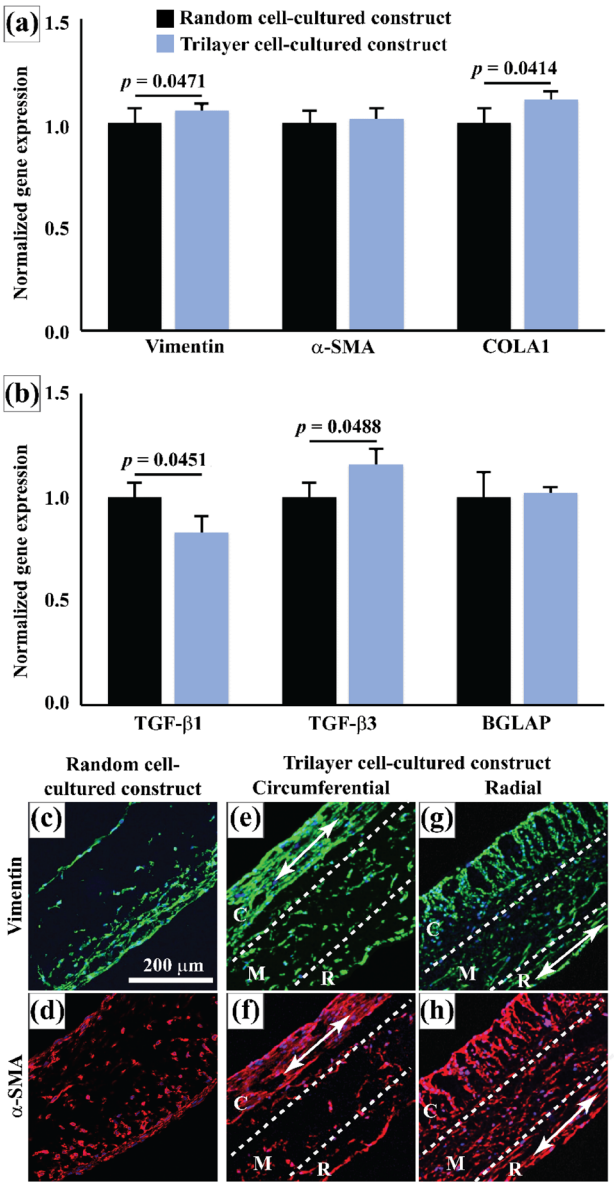

Fig. 6 Measurement of the gene expression of cells in the random and trilayer cell-cultured constructs. **a** Normalized gene expression of vimentin, α-smooth muscle actin (α-SMA), and collagen type I in the cell-cultured constructs. **b** Normalized gene expression of TGF-β1, TGF-β3, and BGLAP in the cell-cultured constructs. **c**, **d** Images of vimentin (**c**) and α-SMA (**d**) protein marker-stained sections of the random fiber cell-cultured construct. **e**–**h** Images of vimentin and α-SMA protein marker-stained circumferentially (**e**, **f**) and radially (**g**, **h**) sectioned cell-cultured constructs with distinct orientations (C, M, and R) of their vimentin protein filaments and α-SMA proteins. Alignment in the circumferential and radial directions can be observed in the C and R layers (shown with a double-headed arrow). Dots in the R layer of the circumferential cross sections and the C layer of the radial cross sections show the alignment perpendicular to the cross section. The random middle (M) layer showed a random orientation. BGLAP: bone gamma-carboxyglutamate protein; C: circumferential layer; R: radial layer

proliferation and ECM production in trilayer cell-cultured constructs than in the random cell-cultured constructs. Thus,

more VICs could have been in a growth state and expressed more α-SMA proteins in the trilayer cell-cultured constructs [17, 71].

Analysis of individual layers

Native heart valve leaflets have a trilayer ECM with distinct cell orientations and gene expression in each layer of the structure [4, 5]. Thus, the circumferential and random/radial layers of the trilayer cell-cultured constructs were separated, and the surfaces were imaged to determine the cell and ECM orientation. Furthermore, the gene expression in the circumferential and random/radial layers was evaluated to determine if the cell gene expression differed throughout the structure. The random/radial layers could not be separated due to the thinness of the radial layer and the strong bond between the two layers. SEM images of the surface of the layers showed an elongated cell morphology along the direction of the fibers in the circumferential and radial layers and no cell elongation in the random layer of the trilayer cell-cultured constructs (Figs. 7a–7c). The confocal immunostaining images of the circumferential, random, and radial surfaces stained with a vimentin marker confirmed that the aligned electrospun fibers in the circumferential and radial layers caused the development of an elongated cell morphology parallel to the direction of the electrospun fiber (Figs. 7d–7f). Additionally, the random layer contained cells without an elongated morphology.

The cells in the random/radial layers showed higher gene expression of vimentin and collagen type I than cells in the circumferential layer; however, there was no difference in α-SMA gene expression in the different layers (Fig. 7g). As shown in the histology section, significantly greater cell proliferation and ECM material production occurred in the circumferential layer than in the random/radial layers of the trilayer cell-cultured constructs. More VICs′ vimentin and collagen expression in the random/radial layers could have indicated that more cells are in a growth state than in the circumferential layer [65, 66]. Furthermore, greater TGF-β3 gene expression by VICs was observed in the random/radial layers than in the circumferential layer, but their TGF-β1 and BGLAP expression levels were similar (Fig. 7h). In native leaflets, the random and radial layers express more TGF-β3 because they are typically softer and more flexible than the circumferential layer [72]. Similarly, in substrates for tissue engineering, the expression of TGF-β3 would be higher in the random/radial layers than in the circumferential layer because they were electrospun with lower PCL concentrations, yielding lower mechanical properties [69]. The low expression (C_p>34) of BGLAP in the random/radial layers and circumferential layer suggests no sign of calcification in any of the trilayer cell-cultured constructs.

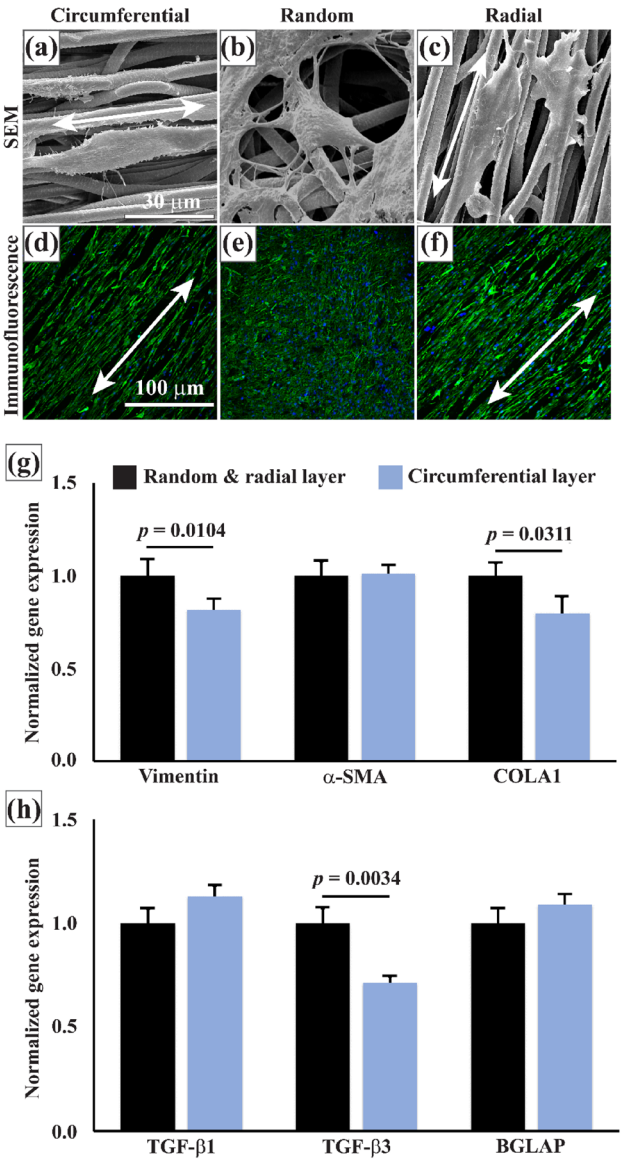

Fig. 7 Cellular proliferation and gene expression in the circumferential, random, and radial layers of the trilayer cell-cultured constructs. **a–c** Scanning electron microscopy (SEM) images of cells in the circumferential (**a**), random (**b**), and radial (**c**) layers of the trilayer cell-cultured constructs with orientations parallel to the fibers (shown with a double-headed arrow). **d–f** Circumferential (**d**), random (**e**), and radial (**f**) surfaces of the trilayer cell-cultured constructs stained for vimentin and Hoechst. The orientations of the cells are shown with a double-headed arrow. **g** Normalized gene expression of vimentin, α-smooth muscle actin (α-SMA), and collagen type I in the circumferential, random, and radial layers of the trilayer cell-cultured constructs. **h** Normalized gene expression of TGF-β1, TGF-β3, and bone gamma-carboxyglutamate protein (BGLAP) in the circumferential, random, and radial layers of the trilayer cell-cultured constructs

This is the first study that compared random substrates to trilayer substrates for heart valve tissue engineering and verified the effects of the trilayer structure on PVICs. Among the two substrates, cell-cultured constructs developed with trilayer substrates had more anisotropic mechanical properties,

more cell proliferation and ECM production, and better gene and protein expression than random cell-cultured constructs. This study established the benefits of developing trilayer leaflet substrates that mimic the structure of native leaflet tissues.

Conclusions

Random and trilayer microfibrous leaflet substrates were produced by electrospinning. Trilayer substrates exhibited higher circumferential and lower radial tensile properties—thus yielding anisotropic characteristics to the substrate—compared to random substrates. PVICs were seeded onto both substrates to produce cell-cultured constructs that were then characterized. While the substrate exhibited similar cell adhesion to the material, cell proliferation was significantly greater in the trilayer cell-cultured constructs than in the random cell-cultured constructs. Protein assays indicated that GAG and collagen quantities were greater in the trilayer cell-cultured constructs than in the random cell-cultured constructs. Furthermore, protein mass spectrometry confirmed that trilayer cell-cultured constructs contained more ACTG1, tubulin, PGK-1, histones, collagen type I & III, and vimentin proteins than random cell-cultured constructs. The PVICs in trilayer cell-cultured constructs showed increased expression of vimentin, collagen, TGF-β1, and TGF-β3. These results demonstrated that the trilayer structure and anisotropic mechanical properties positively impact the PVICs and the produced ECM. Additionally, analysis of the trilayer cell-cultured constructs indicated that the VICs expressed more vimentin, collagen, and TGF-β3 in the random/radial layers than in the circumferential layer of the constructs. These observations suggest that the layers of the trilayer construct influence cell phenotypes and gene expression.

Acknowledgements This work was supported by the National Institute of Health (No. NIH R00HL134823).

Author contributions YS was involved in data curation, formal analysis, investigation, visualization, and writing—original draft. SJ was involved in funding acquisition, project administration, conceptualization, analysis, and writing—review and editing.

Declarations

Conflict of interest The authors declare that they have no conflict of interest.

Ethical approval This article does not contain any studies with human or animal subjects performed by any of the authors.

Data availability The raw data required to reproduce these findings cannot be shared at this time as the data also form part of an ongoing study. The processed data (used in this manuscript) required to reproduce these findings can be shared at this time through personal request.

References

1. Coffey S, Roberts-Thomson R, Brown A et al (2021) Global epidemiology of valvular heart disease. Nat Rev Cardiol 18:853–864. https://doi.org/10.1038/s41569-021-00570-z
2. Zandi S, Imani B, Safarpor G et al (2021) Self-management of patients with heart valve replacement and its clinical outcomes: a systematic review. Polish J Cardio Thorac Surg 18(1):40–49. https://doi.org/10.5114/kitp.2021.105186
3. Fioretta ES, Motta SE, Lintas V et al (2020) Next-generation tissue-engineered heart valves with repair, remodelling and regeneration capacity. Nat Rev Cardiol 18:92–116. https://doi.org/10.1038/s41569-020-0422-8
4. Chen Q, Bruyneel A, Carr C et al (2020) Trilayer scaffold with cardiosphere-derived cells for heart valve tissue engineering. J Biomed Mater Res Part B Appl Biomater 108(3):729–737. https://doi.org/10.1002/jbm.b.34427
5. Simionescu DT, Chen J, Jaeggli M et al (2012) Form follows function: advances in trilayered structure replication for aortic heart valve tissue engineering. J Healthc Eng 3(2):179–202. https://doi.org/10.1260/2040-2295.3.2.179
6. Schroeder ME, Rodriguez AG, Speckl KF et al (2021) Collagen networks within 3D PEG hydrogels support valvular interstitial cell matrix mineralization. Acta Biomater 119:197–210. https://doi.org/10.2139/ssrn.3677406
7. Sanz CG, Mihaila AC, Evanghelidis A et al (2022) Quantification of cell oxygenation in 2D constructs of metallized electrospun polycaprolactone fibers encapsulating human valvular interstitial cells. J Electroanal Chem 905:116005. https://doi.org/10.1016/j.jelechem.2021.116005
8. Wu S, Li Y, Zhang C et al (2022) Tri-layered and gel-like nanofibrous scaffolds with anisotropic features for engineering heart valve leaflets. Adv Healthc Mater 11(10):2200053. https://doi.org/10.1002/adhm.202200053
9. Scott AJ, Simon LR, Hutson HN et al (2021) Engineering the aortic valve extracellular matrix through stages of development, aging, and disease. J Mol Cell Cardiol 161:1–8. https://doi.org/10.1016/j.yjmcc.2021.07.009
10. Emmert MY, Schmitt BA, Loerakker S et al (2018) Computational modeling guides tissue-engineered heart valve design for long-term in vivo performance in a translational sheep model. Sci Transl Med 10(440):eaan4587. https://doi.org/10.1126/scitranslmed.aan4587
11. Syedain ZH, Bradee AR, Kren S et al (2013) Decellularized tissue-engineered heart valve leaflets with recellularization potential. Tissue Eng Part A 19(5–6):759–769. https://doi.org/10.1089/ten.tea.2012.0365
12. Uiterwijk M, Smits AI, van Geemen D et al (2020) In situ remodeling overrules bioinspired scaffold architecture of supramolecular elastomeric tissue-engineered heart valves. JACC Basic Transl Sci 5:1187–1206. https://doi.org/10.1016/j.jacbts.2020.09.011
13. Masoumi N, Annabi N, Assmann A et al (2014) Tri-layered elastomeric scaffolds for engineering heart valve leaflets. Biomaterials 35(27):7774–7785. https://doi.org/10.1016/j.biomaterials.2014.04.039

14. Tseng H, Cuchiara ML, Durst CA et al (2013) Fabrication and mechanical evaluation of anatomically-inspired quasilaminate hydrogel structures with layer-specific formulations. Ann Biomed Eng 41(2):398–407. https://doi.org/10.1007/s10439-012-0666-5
15. Wu S, Dong T, Li Y et al (2022) State-of-the-art review of advanced electrospun nanofiber yarn-based textiles for biomedical applications. Appl Mater Today 27:101473. https://doi.org/10.1016/j.apmt.2022.101473
16. Wu S, Kumar V, Xiao P et al (2020) Age related extracellular matrix and interstitial cell phenotype in pulmonary valves. Sci Rep 10:21338. https://doi.org/10.1038/s41598-020-78507-8
17. Jana S, Lerman A (2019) Behavior of valvular interstitial cells on trilayered nanofibrous substrate mimicking morphologies of heart valve leaflet. Acta Biomater 85:142–156. https://doi.org/10.1016/j.actbio.2018.12.005
18. Jana S, Franchi F, Lerman A (2019) Trilayered tissue structure with leaflet-like orientations developed through in vivo tissue engineering. Biomed Mater 15(1):015004. https://doi.org/10.1088/1748-605x/ab52e2
19. Jana S, Lerman A (2020) In vivo tissue engineering of a trilayered leaflet-shaped tissue construct. Regener Med 15(1):1177–1192. https://doi.org/10.2217/rme-2019-0078
20. Snyder Y, Jana S (2022) Anisotropicity and flexibility in trilayered microfibrous substrates promote heart valve leaflet tissue engineering. Biomed Mater 17(6):065013. https://doi.org/10.1088/1748-605x/ac94ae
21. Snyder Y, Jana S (2022) Strategies for development of decellularized heart valve scaffolds for tissue engineering. Biomaterials 288:121675. https://doi.org/10.1016/j.biomaterials.2022.121675
22. Zakko J, Blum KM, Drews JD et al (2020) Development of tissue engineered heart valves for percutaneous transcatheter delivery in a fetal ovine model. Basic Transl Sci 5(8):815–828. https://doi.org/10.1016/j.jacbts.2020.06.009
23. Jana S, Bhagia A, Lerman A (2019) Optimization of polycaprolactone fibrous scaffold for heart valve tissue engineering. Biomed Mater 14(6):065014. https://doi.org/10.1088/1748-605x/ab3d24
24. Walsh M, Cunnane E, Mulvihill J et al (2014) Uniaxial tensile testing approaches for characterisation of atherosclerotic plaques. J Biomech 47(4):793–804. https://doi.org/10.1016/j.jbiomech.2014.01.017
25. Engelmayr Jr GC, Hildebrand DK, Sutherland FW et al (2003) A novel bioreactor for the dynamic flexural stimulation of tissue engineered heart valve biomaterials. Biomaterials 24(14):2523–2532. https://doi.org/10.1016/s0142-9612(03)00051-6
26. Gloeckner DC, Billiar KL, Sacks MS (1999) Effects of mechanical fatigue on the bending properties of the porcine bioprosthetic heart valve. ASAIO J 45(1):59–63. https://doi.org/10.1097/00002480-199901000-00014
27. Santa C, Anjo SI, Manadas B (2016) Protein precipitation of diluted samples in SDS-containing buffer with acetone leads to higher protein recovery and reproducibility in comparison with TCA/acetone approach. Proteomics 16(13):1847–1851. https://doi.org/10.1002/pmic.201600024
28. Wilkinson J (1986) Fragmentation of polypeptides by enzymic methods. In: Darbre A (Ed.), Practical Protein Chemistry: a Handbook. John Wiley and Sons, New York, NY, USA
29. Zhang J, Xin L, Shan B et al (2012) PEAKS DB: de novo sequencing assisted database search for sensitive and accurate peptide identification. Mol Cell Proteomics 11(4):M111.010587. https://doi.org/10.1074/mcp.m111.010587
30. Blake RR, Markby GR, Culshaw GJ et al (2020) Survival of activated myofibroblasts in canine myxomatous mitral valve disease and the role of apoptosis. Res Vet Sci 128:99–106. https://doi.org/10.1016/j.rvsc.2019.11.004
31. Hasan A, Soliman S, El Hajj F et al (2018) Fabrication and in vitro characterization of a tissue engineered PCL-PLLA heart valve. Sci Rep 8:8187. https://doi.org/10.1038/s41598-018-26452-y
32. Tseng H, Grande-Allen KJ (2009) Microstructure of the aortic valve: implications for valvular mechanics and function. In: Schmitt L, Konig T (Eds.), Advances in Cardiovascular Research. Nova Science Publishers, Hauppauge, NY, USA
33. Baji A, Mai YW, Wong SC et al (2010) Electrospinning of polymer nanofibers: effects on oriented morphology, structures and tensile properties. Compos Sci Technol 70(5):703–718. https://doi.org/10.1016/j.compscitech.2010.01.010
34. Pina S, Ribeiro VP, Marques CF et al (2019) Scaffolding strategies for tissue engineering and regenerative medicine applications. Materials 12(11):1824. https://doi.org/10.3390/ma12111824
35. Uhal BD, Ramos C, Joshi I et al (1998) Cell size, cell cycle, and α-smooth muscle actin expression by primary human lung fibroblasts. Am J Phys-Lung Cellular Mol Physiol 275(5):L998–L1005. https://doi.org/10.1152/ajplung.1998.275.5.l998
36. Ragaert K, De Somer F, Somers P et al (2012) Flexural mechanical properties of porcine aortic heart valve leaflets. J Mech Behavior Biomed Mater 13:78–84. https://doi.org/10.1016/j.jmbbm.2012.04.009
37. Buchanan RM, Sacks MS (2014) Interlayer micromechanics of the aortic heart valve leaflet. Biomech Model Mechanobiol 13(4):813–826. https://doi.org/10.1007/s10237-013-0536-6
38. Sacks MS, Merryman WD, Schmidt DE (2009) On the biomechanics of heart valve function. J Biomech 42(12):1804–1824. https://doi.org/10.1016/j.jbiomech.2009.05.015
39. Wu S, Duan B, Qin X et al (2017) Living nano-micro fibrous woven fabric/hydrogel composite scaffolds for heart valve engineering. Acta Biomater 51:89–100. https://doi.org/10.1016/j.actbio.2017.01.051
40. Panwar P, Lamour G, Mackenzie NC et al (2015) Changes in structural-mechanical properties and degradability of collagen during aging-associated modifications. J Biol Chem 290(38):23291–23306. https://doi.org/10.1074/jbc.m115.644310
41. Kalejs M, Stradins P, Lacis R et al (2009) St Jude Epic heart valve bioprostheses versus native human and porcine aortic valves–comparison of mechanical properties. Interact Cardiovasc Thorac Surg 8(5):553–556. https://doi.org/10.1510/icvts.2008.196220
42. Amoroso NJ, D'Amore A, Hong Y et al (2012) Microstructural manipulation of electrospun scaffolds for specific bending stiffness for heart valve tissue engineering. Acta Biomater 8(12):4268–4277. https://doi.org/10.1016/j.actbio.2012.08.002
43. Li Y, Meng H, Liu Y et al (2015) Fibrin gel as an injectable biodegradable scaffold and cell carrier for tissue engineering. Sci World J 2015:685690. https://doi.org/10.1155/2015/685690
44. Mol A, van Lieshout MI, Dam-de Veen CG et al (2005) Fibrin as a cell carrier in cardiovascular tissue engineering applications. Biomaterials 26(16):3113–3121. https://doi.org/10.1016/j.biomaterials.2004.08.007
45. Kim JI, Hwang TI, Aguilar LE et al (2016) A controlled design of aligned and random nanofibers for 3D bi-functionalized nerve conduits fabricated via a novel electrospinning set-up. Sci Rep 6:23761. https://doi.org/10.1038/srep23761
46. Muzzio N, Moya S, Romero G (2021) Multifunctional scaffolds and synergistic strategies in tissue engineering and regenerative medicine. Pharmaceutics 13(6):792. https://doi.org/10.3390/pharmaceutics13060792
47. Thrivikraman G, Jagiełło A, Lai VK et al (2021) Cell contact guidance via sensing anisotropy of network mechanical resistance. Proc Natl Acad Sci USA 118(29):e2024942118. https://doi.org/10.1073/pnas.2024942118
48. Chen L, Yan C, Zheng Z (2018) Functional polymer surfaces for controlling cell behaviors. Mater Today 21(1):38–59. https://doi.org/10.1016/j.mattod.2017.07.002

49. Hannan RT, Peirce SM, Barker TH (2017) Fibroblasts: diverse cells critical to biomaterials integration. ACS Biomater Sci Eng 4(4):1223–1232. https://doi.org/10.1021/acsbiomaterials.7b00244
50. Nerurkar NL, Sen S, Baker BM et al (2011) Dynamic culture enhances stem cell infiltration and modulates extracellular matrix production on aligned electrospun nanofibrous scaffolds. Acta Biomater 7(2):485–491. https://doi.org/10.1016/j.actbio.2010.08.011
51. Jana S, Lerman A, Simari RD (2015) In vitro model of a fibrosa layer of a heart valve. ACS Appl Mater Interfaces 7(36):20012–20020. https://doi.org/10.1021/acsami.5b04805
52. McCullen SD, Autefage H, Callanan A et al (2012) Anisotropic fibrous scaffolds for articular cartilage regeneration. Tissue Eng Part A 18(19–20):2073–2083. https://doi.org/10.1089/ten.tea.2011.0606
53. Jana S, Franchi F, Lerman A (2021) Fibrous heart valve leaflet substrate with native-mimicked morphology. Appl Mater Today 24:101112. https://doi.org/10.1016/j.apmt.2021.101112
54. Kodigepalli KM, Thatcher K, West T et al (2020) Biology and biomechanics of the heart valve extracellular matrix. J Cardiovasc Dev Disease 7(4):57. https://doi.org/10.3390/jcdd7040057
55. Nachlas AL, Li S, Streeter BW et al (2020) A multilayered valve leaflet promotes cell-laden collagen type I production and aortic valve hemodynamics. Biomaterials 240:119838. https://doi.org/10.1016/j.biomaterials.2020.119838
56. Fraley SI, Wu PH, He L et al (2015) Three-dimensional matrix fiber alignment modulates cell migration and MT1-MMP utility by spatially and temporally directing protrusions. Sci Rep 5:14580. https://doi.org/10.1038/srep14580
57. Sundby LJ, Southern WM, Hawbaker KM et al (2022) Nucleotide- and protein-dependent functions of Actg1. Mol Biol Cell 33(9):ar77. https://doi.org/10.1091/mbc.e22-02-0054
58. Moore K, Moore R, Wang C et al (2020) Tugging at the heart strings: the septin cytoskeleton in heart development and disease. J Cardiovasc Dev Disease 7(1):3. https://doi.org/10.3390/jcdd7010003
59. Gibb AA, Lazaropoulos MP, Elrod JW (2020) Myofibroblasts and fibrosis: mitochondrial and metabolic control of cellular differentiation. Circ Res 127(3):427–447. https://doi.org/10.1161/circresaha.120.316958
60. Gu J, Lu Y, Deng M et al (2019) Inhibition of acetylation of histones 3 and 4 attenuates aortic valve calcification. Exp Mol Med 51(7):1–14. https://doi.org/10.1038/s12276-019-0272-9
61. Augière C, Mégy S, El Malti R et al (2015) A novel alpha cardiac actin (ACTC1) mutation mapping to a domain in close contact with myosin heavy chain leads to a variety of congenital heart defects, arrhythmia and possibly midline defects. PLoS ONE 10(6):e0127903. https://doi.org/10.1371/journal.pone.0127903
62. Greco RM, Iocono JA, Ehrlich HP (1998) Hyaluronic acid stimulates human fibroblast proliferation within a collagen matrix. J Cell Physiol 177(3):465–473. https://doi.org/10.1002/(sici)1097-4652(199812)177:3%3c465::aid-jcp9%3e3.0.co;2-5
63. Kim YS, Kim MJ, Koo TH et al (2012) Histone deacetylase is required for the activation of Wnt/β-catenin signaling crucial for heart valve formation in zebrafish embryos. Biochem Biophys Res Commun 423(1):140–146. https://doi.org/10.1016/j.bbrc.2012.05.098
64. Duan B, Yin Z, Kang LH et al (2016) Active tissue stiffness modulation controls valve interstitial cell phenotype and osteogenic potential in 3D culture. Acta Biomater 36:42–54. https://doi.org/10.1016/j.actbio.2016.03.007
65. Quinlan AMT, Billiar KL (2012) Investigating the role of substrate stiffness in the persistence of valvular interstitial cell activation. J Biomed Mater Res Part A 100(9):2474–2482. https://doi.org/10.1002/jbm.a.34162
66. Porras AM, van Engeland NC, Marchbanks E et al (2017) Robust generation of quiescent porcine valvular interstitial cell cultures. J Am Heart Assoc 6(3):e005041. https://doi.org/10.1161/jaha.116.005041
67. Liu AC, Gotlieb AI (2008) Transforming growth factor-β regulates in vitro heart valve repair by activated valve interstitial cells. Am J Pathol 173(5):1275–1285. https://doi.org/10.2353/ajpath.2008.080365
68. Semenova D, Zabirnyk A, Lobov A et al (2022) Investigation of transcriptional changes underlying calcification of aortic valve. Cardiovasc Res 118(Supplement_1):cvac066.140. https://doi.org/10.1093/cvr/cvac066.140
69. Lichtman MK, Otero-Vinas M, Falanga V (2016) Transforming growth factor beta (TGF-β) isoforms in wound healing and fibrosis. Wound Repair Regener 24(2):215–222. https://doi.org/10.1111/wrr.12398
70. Mendez MG, Kojima SI, Goldman RD (2010) Vimentin induces changes in cell shape, motility, and adhesion during the epithelial to mesenchymal transition. FASEB J 24(6):1838–1851. https://doi.org/10.1096/fj.09-151639
71. Jana S, Morse D, Lerman A (2021) Leaflet tissue generation from microfibrous heart valve leaflet scaffolds with native characteristics. ACS Appl Bio Mater 4(11):7836–7847. https://doi.org/10.1021/acsabm.1c00768
72. Goumans MJ, Ten Dijke P (2018) TGF-β signaling in control of cardiovascular function. Cold Spring Harbor Perspect Biol 10(2):a022210. https://doi.org/10.1101/cshperspect.a022210